Flexible magnesium-ion-conducting solid poly-blend electrolyte films for magnesium-ion batteries

Pradeep Nayak[1], Ismayil[1,*] , Y. N. Sudhakar[2], and M. S. Murari[3]

[1] *Department of Physics, Manipal Institute of Technology, Manipal Academy of Higher Education, Manipal 576104, Karnataka, India*
[2] *Department of Chemistry, Manipal Institute of Technology, Manipal Academy of Higher Education, Manipal 576104, Karnataka, India*
[3] *Nanoscience Research Laboratory, Department of Physics, NITTE (Deemed to Be University), NMAM Institute of Technology, Nitte, Karkala 574110, Karnataka, India*

ABSTRACT

Solid biodegradable polymer electrolyte systems are considered the optimal choice for energy storage devices because they are both cost-effective and energy-efficient. A solid blend polymer electrolyte (SBPE) membrane capable of transporting magnesium ions was prepared using a mixture of 70 wt% methylcellulose, 30 wt% chitosan, and varying wt% magnesium perchlorate salt. X-ray diffraction analysis revealed an increase in the amorphous nature caused by the inclusion of $Mg(ClO_4)_2$ salt in the polymer blend matrix. A Fourier transform infrared spectroscopy study of samples containing varying salt concentrations revealed secondary interactions between polymer segments and salt, which provides the basis for energy density. Moreover, through impedance analysis, it was determined that the bulk resistance decreased with increasing salt concentration. The SBPE containing 30 wt% magnesium perchlorate exhibited the highest ionic conductivity, with a value of 2.49×10^{-6} S cm^{-1}. A comprehensive evaluation of the ion transport parameters, including mobility, carrier density, and diffusion, was conducted for the prepared electrolyte samples. Notably, an ionic transference number (t_{ion}) of approximately 0.83 was observed for the SBPE sample with 30 wt% magnesium salt, indicating ions' prevalence as the system's primary charge carriers. Electrochemical analyses demonstrated that the SBPE with the highest ion conductivity possessed an electrochemical stability window (ESW) of 1.92 V. Additionally, the thermal characteristics of the samples were evaluated using thermogravimetric analysis (TGA) to assess the thermal stability of the electrolyte. Finally, the highest conducting polymer electrolyte was employed to construct a primary magnesium battery, and its discharge profile with different cathode materials was studied. Based on these findings, the current study suggests an environmentally friendly, biodegradable, and economically viable electrolyte option suitable for separator cum electrolytes in magnesium-ion batteries.

Address correspondence to E-mail: ismayil.mit@manipal.edu; ismayil.486@gmail.com

Springer

1 Introduction

Over 85% of our energy requirements are met by fossil fuels, which significantly contribute to greenhouse gas emissions, global warming, and economic challenges [1]. In the coming years, because of energy shortages and environmental pollution, we will encounter numerous challenges in transitioning communities from nonrenewable energy systems to renewable sources [2, 3]. This underscores the importance of the scientific community exploring sustainable alternative energy options that align with Sustainable Development Goal 7, which aims for affordable and clean energy access for all. Both natural and synthetic polymers have been commonly employed in synthesizing solid blend polymer electrolytes (SBPEs) for optical and energy-storing device applications [4]. With the increasing use of electronic devices leading to significant electronic waste disposal, researchers are exploring biodegradable materials as substitutes for nonbiodegradable devices. Biodegradable polymers offer unique features, such as their abundance, nontoxic nature, easy processing, and cost-effectiveness, making them attractive alternatives [5]. Chitosan, carrageenan, tamarind seeds, starch, and agar are commonly used biopolymers to prepare SBPE for electrochemical devices [6]. For three to four decades, these biopolymer electrolytes have been extensively used in batteries [7], electrical double-layer capacitors (EDLCs) [8], supercapacitors, photovoltaic cells [9], and dye-sensitized solar cells (DSSCs) [10]. Significant research efforts have been dedicated to liquid electrolytes for energy storage applications because they produce high ionic conductivity, while relatively less attention has been given to solid biopolymer electrolytes [11]. While liquid electrolytes offer high ionic conductivity, SBPE provides the advantage of being leak-proof and allows for more compact device designs [12]. Prioritizing environmentally friendly energy storage devices is essential to balance the growing demand and environmental impact.

Combining various inorganic salts with polar polymers can alter their physical and chemical characteristics. Chitosan has been widely used as a polymer host base to incorporate high levels of salts such as H^+, Li^+, and Na^+, making the resulting film more rigid [13]. Chitosan (CS) has very low conductivity in its actual state, and to make it conduct, we must add some inorganic salts [14]. Methylcellulose (MC) is an abundant, naturally occurring, biodegradable, renewable

polymer [5]. Less work has been done on magnesium (Mg)-based salts. Magnesium-based salts offer benefits such as abundance, ease of handling, and no dendrite growth [16]. The ionic conductivity is a crucial parameter for energy storage device applications.

Several techniques, such as adding additives, copolymerization, and blending, have been adopted to achieve desirable ionic conduction at ambient temperatures [17]. Blends are physical mixtures of two or more polymers with various structural properties that interact with one another via secondary forces and noncovalent bonding [18]. Blending polymers are widely used for developing new materials due to their ease of formulation and ability to control material properties [19].

Abdalrahman et al. [20] used NaSCN salt to synthesize SBPE films using MC as a polymer host and obtained a conductivity of 3.6×10^{-6} S cm^{-1}. Ahmed et al. [21] used LiBF$_4$ as a salt to formulate an SBPE film of CS:MC and obtained a conductivity of 2.12×10^{-5} S cm^{-1}. Using ammonium nitrate as a salt, S. Abdulkareem synthesized a blend polymer electrolyte film of CS:MC and achieved a conductivity of 3.54×10^{-4} S cm^{-1} [22]. O. Abdullah et al. [23] used CS:MC as a poly-blend, incorporated LiI salt, and reported a conductivity of 6.26×10^{-6} S cm^{-1}. Figure 1 shows the ambient temperature ionic conductivity and ESW of the optimum SBPE films based on chitosan, methylcellulose, CS:MC poly-blend, and other polymers doped with Mg(ClO$_4$)$_2$. There are very few studies on CS:MC
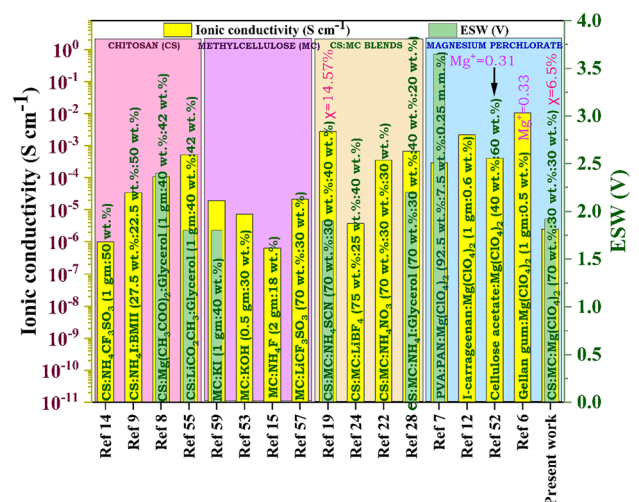
Fig. 1 Previous research on chitosan, methylcellulose, CS:MC SBPE, and magnesium perchlorate salt, along with the ideal polymer electrolyte's room-temperature conductivity and ESW

SBPE doped with Mg salts, and no attempt has been made to examine the impact of $Mg(ClO_4)_2$ salt doping on CS:MC blends for use in Mg batteries. Hence, this study focused on developing and characterizing SBPEs based on chitosan and methylcellulose. Methylcellulose and chitosan are derived from cellulose and chitin, respectively, and have attracted the attention of many researchers worldwide because of their exceptional properties, such as abundance, water solubility, compatibility with different solvents, and outstanding film-forming capacity [24]. According to our earlier work [25], the most amorphous blend matrix, i.e., 30 wt% MC and 70 wt% CS, was used as the host polymer matrix to synthesize the magnesium ion-conducting biopolymer electrolyte.

In this work, various amounts of magnesium perchlorate were incorporated into a CS:MC blend matrix to study the performance of the electrolytes. The uniqueness of our work is that we have incorporated deconvolution of XRD for all these electrolytes to understand the percentage crystallinity and thereby predict the conductivity trend. Moreover, we found that very few articles have discussed the transport properties of magnesium ions, especially in blended polymer electrolytes. As the blend possesses different functional groups in its matrix, the magnesium ions interact with them during its movement, which certainly has a different trend from that of sodium/lithium ions. The challenge of using Mg^{2+}, which has bivalency and tends to be more attractive toward polymer segments, has been addressed in this paper. The nature and mechanism of charge transfer in these materials are thought to be revealed by studying their electrochemical characteristics.

2 Materials and instrumentation

2.1 Solid blend polymer electrolyte (SBPE) preparation

Chitosan (CS), methylcellulose (MC), and $Mg(ClO_4)_2$ are the materials employed in the present study, and they were all purchased from Loba Chemie Pvt Ltd. SBPE was synthesized using double-distilled water, and analytical grade acetic acid was obtained from S.D. Fine-Chem Pvt. Limited in Mumbai, India. The solution casting method was used to develop the SBPE comprising $CS:MC:Mg(ClO_4)_2$. The preparation of the SBPE samples followed our earlier research

[26]. A series of SBPEs (70 wt% CS/30 wt% MC + x wt% $Mg(ClO_4)_2$, where $x = 0$ to 30 wt% in steps of 5 wt%) were prepared. In the present work, the total weight of all the components (polymers and the dopant) was fixed to 2 g. An appropriate amount of optimized polymer blend (70 wt% of CS/30 wt% of MC) and $Mg(ClO_4)_2$ salt with $x = 0$, 5, 10, 15, 20, 25, and 30 wt.% were dissolved separately in 100 ml of 1% acetic acid solution under continuous stirring at 40 °C for 7 to 8 h until a homogeneous viscous solution was obtained and labeled CMP0, CMP5, CMP10, CMP15, CMP20, CMP25, and CMP30, respectively. The thickness of the synthesized films ranged from 171 to 238 μm. Table 1 provides the weight percentages of the polymers and salt components used in the study.

A primary electrochemical cell consisting of an Mg (anode)/(CS-MC-$Mg(ClO_4)_2$) (70–30-30)/(cathode) configuration was assembled, employing the most conductive SBPE film, and the cell performance was examined. A magnesium metal piece with a 13 mm diameter was utilized for anode preparation. In terms of cathode preparation, a combination of MnO_2, graphite (C), and CMP30 SBPE was mixed to produce a pellet with a 13 mm diameter (designated cell 1). Another pellet was created by mixing iodine (I_2), C, and CMP30 SBPE, which was then compressed under a 5-ton pressure (designated cell 2). The third pellet was formed by mixing V_2O_5, C, and CMP30 SBPE (designated cell 3). One more pellet was formed by mixing PbO_2, V_2O_5, C, and CMP30 SBPE (designated cell 4). All these pellets were used to assess the performance of the primary battery.

Table 1 Sample label and wt% of each constituent of the polymer blend

Sample designation	Polymer chitosan (g)	Polymer methylcellulose (g)	Dopant $Mg(ClO_4)_2$ (g)
CMP0	1.44	0.56	–
CMP5	1.33	0.57	0.10
CMP10	1.26	0.54	0.20
CMP15	1.19	0.51	0.30
CMP20	1.12	0.48	0.40
CMP25	1.05	0.45	0.50
CMP30	0.98	0.42	0.60

2.2 Characterization

A Rigaku Miniflex 600 instrument (5th Gen.) was used for X-ray diffraction (XRD) analysis of the SBPE samples. With a step size of 0.02°, the experiments were performed utilizing monochromatic Cu K-alpha radiation with a wavelength of 1.54 Å and glancing angles ranging from 5° to 80°.

The FTIR spectrum profiles were obtained using a Shimadzu IR Spirit ATR-FTIR spectrophotometer, with infrared beams passed through the samples at ambient temperature. The spectra were acquired in transmittance mode with a resolution of 4 cm^{-1} and a wavenumber range of 400–4000 cm^{-1}.

The surface morphology of the polymer electrolyte film was examined by scanning electron microscopy (CARL ZESIS) at 1000 × magnification.

The thermal stability of solid polymer electrolyte films was studied using an SDT Q600 V20.9 instrument 20.

Electrical impedance spectroscopy (EIS) is a suitable method for understanding the electrical properties of SBPE. Before impedance analysis, the SBPE samples were cut into small pieces with a contact area of 1.44 cm^2 and then pressed between two silver-blocking electrodes using spring pressure. An impedance study used an LCR meter in the 100 Hz to 5 MHz frequency range. The software was utilized to extract various parameters, such as the parallel capacitance (C), real part (Z_r), and imaginary part (Z_i), of the complex impedance spectra of the electrochemical impedance spectroscopy (EIS) plots. By identifying the point where the plot intersects the real axis, the bulk resistance (R_b) was determined [22]. Equation (1) was utilized to determine the electrolyte films' ionic conductivity at ambient temperature based on the R_b value [27].

$$\sigma = \frac{t}{AR_b} \tag{1}$$

The complex permittivity illustrates the trends of dielectric relaxation in solid polymers.

$$\varepsilon^*(\omega) = \varepsilon\prime(\omega) - j\varepsilon\prime\prime(\omega) \tag{2}$$

The ion transport properties, such as carrier concentration (n), diffusion coefficient (D), and mobility (μ), were evaluated using the Nyquist plot fitting technique.

The ESW of the SBPE was determined using a Keithley source meter unit (SMU) 2636B. Transference number measurements (TNMs) were performed utilizing a DC polarization technique, wherein the changes in polarization current were monitored over time to assess variations. The cell was polarized using a Keithley SMU 2636B at 0.5 V. For both voltage stability and TNM, the cell arrangement is shown in Fig. 9. t_{ion} can be calculated if the initial (I_i) and steady-state (I_{ss}) currents are known utilizing the below-mentioned equation[19]:

$$t_{ion} = \frac{I_i - I_{ss}}{I_i} \tag{3}$$

The electronic transference number can be calculated using the following equation:

$$t_{elec} = 1 - t_{ion} \tag{4}$$

The voltage stability of the polymer electrolyte was tested using a Keithley source meter 2636B. The cell arrangement was [stainless steel | polymer electrolyte sample | stainless steel].

A cyclic voltammogram was generated using a potentiostat (Biologic) SP50e by sandwiching the highest conducting polymer electrolyte between two magnesium electrodes and two stainless steel electrodes separately at a scan rate of 100 mV s^{-1}.

3 Results and discussion

3.1 XRD analysis

Figure 2 shows the X-ray diffractograms of the CS:MC blend polymer electrolytes with different salt contents. The XRD pattern of MC exhibits a hallow peak in the diffraction angle range between 19° and 21° due to intra/intermolecular hydrogen bonding[28]. Inter- and intramolecular hydrogen bonding between the hydroxyl groups of individual monomers and chains within the CS polymer resulted in XRD peaks at approximately 2θ = 11.3°, 18.3°, and 22.8° [19].

According to the diffractogram, CMP0 consists of two concave peaks, one at approximately 11° and the other at approximately 21°. The appearance of more crystalline peaks in the blended system is due to the greater content of CS over MC. The broad peak at approximately 21° suggested that the CS:MC polyblend had an amorphous composition [29]. Blending
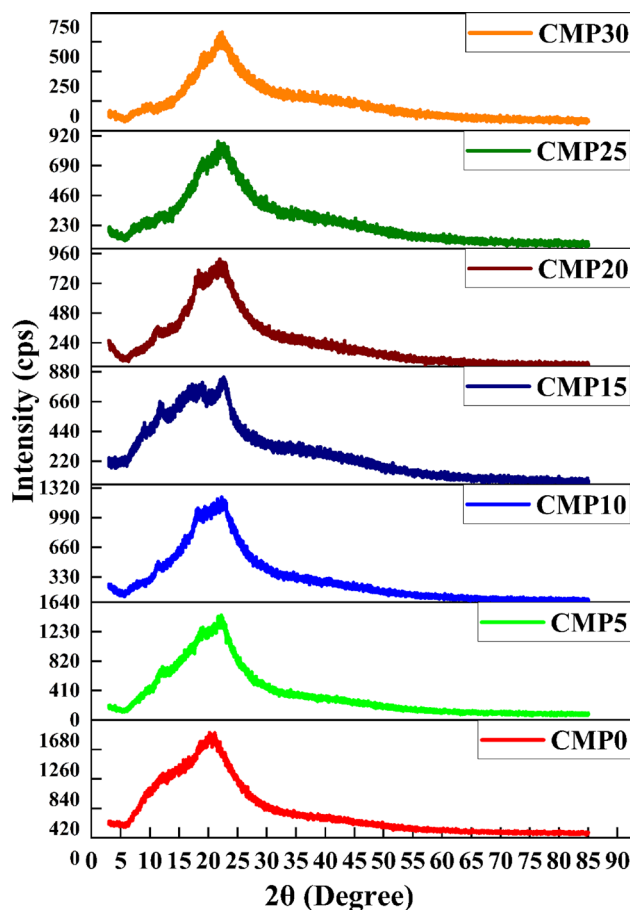
Fig. 2 X-ray diffraction patterns of the prepared poly-blend electrolyte films

plays a crucial role in decreasing crystallinity and subsequently enhancing conductivity [30]. As Abdullah et al. [31] reported that blending CS and MC triggered a decrease in the crystallinity of the blended system. An increase in the broadness and a decrease in the intensity of the peaks imply a decrease in crystallinity, thus providing a lower energy barrier for ion conduction [32]. According to Hodge et al.'s criterion [18], peak intensity reduction and peak broadening compared to those of the pristine polymer indicate the dominance of the amorphous state within a biopolymer blend electrolyte system[33, 34].

The X-ray diffraction peaks were analyzed using Fityk computer software and deconvoluted based on Eq. (5) below [35], as shown in Fig. 3a–g. X-ray diffractograms showed a decrease in crystallinity with increasing salt content, indicating a more amorphous composition in the blended system. The deconvolution of the XRD patterns provided insights into the

percentage of crystallinity, which can be used to predict the conductivity trend.

$$X_C = \frac{A_c}{A_a + A_c} 100\% \qquad (5)$$

3.2 Fourier transform infrared spectroscopy

The FTIR spectra shown in Fig. 4a and b can be used to understand the chemical identity, complex formation, and interactions between the biopolymer electrolyte's different components. The complexation between the blend and the magnesium salt was indicated by shifts in the bands, broadening, and the emergence or disappearance of peaks [36]. The main advantage of polymer blending is that it provides additional complexation sites for the ions to hop or drift, thereby increasing the conductivity [37]. The peak near 2900 cm^{-1} matches the C-H stretching mode of the CMP0-poly-blend system [38], and as the salt concentration increases (CMP5-CMP30), a shift in the peak toward a lower wavenumber is observed due to hydrogen bonding between the oxygen of the perchlorate anion and the hydrogen of C-H. Between 1600 and 1700 cm^{-1}, there is an absorption band corresponding to the stretching of C = O [39], and the intensity of this peak also decreases with the addition of a higher concentration of salt due to the interaction of cations with oxygen. The other modes, centered between 1500 and 1600 cm^{-1}, are N–H bending modes [40]. Figure 4a illustrates how adding salt to the biopolymer blend system caused the peak centered at 3357 cm^{-1}, which was previously identified as -OH stretching, to shift to lower wavenumbers, demonstrating the physical interactions between the salt's magnesium ions and the biopolymer blend [41]. The C-O bending vibration peak was approximately 1057 cm^{-1}, and the C-O stretching vibration peak was approximately 1026 cm^{-1} [15]. The various stretching and bending vibrations are tabulated in Table 2. The peak shift toward lower wavenumbers in the bands corresponding to C-H and C = O stretching vibrations provides compelling evidence of interactions between the biopolymer blend and the magnesium salt [24].

Figure 5 illustrates the potential interaction between the Mg(ClO$_4$)$_2$ salt and the polymer blend. Mg^{2+} acts as a Lewis acid, and ClO^{4-} acts as a Lewis

Fig. 3 a–g XRD deconvoluted pattern for different solid poly-blend electrolyte systems
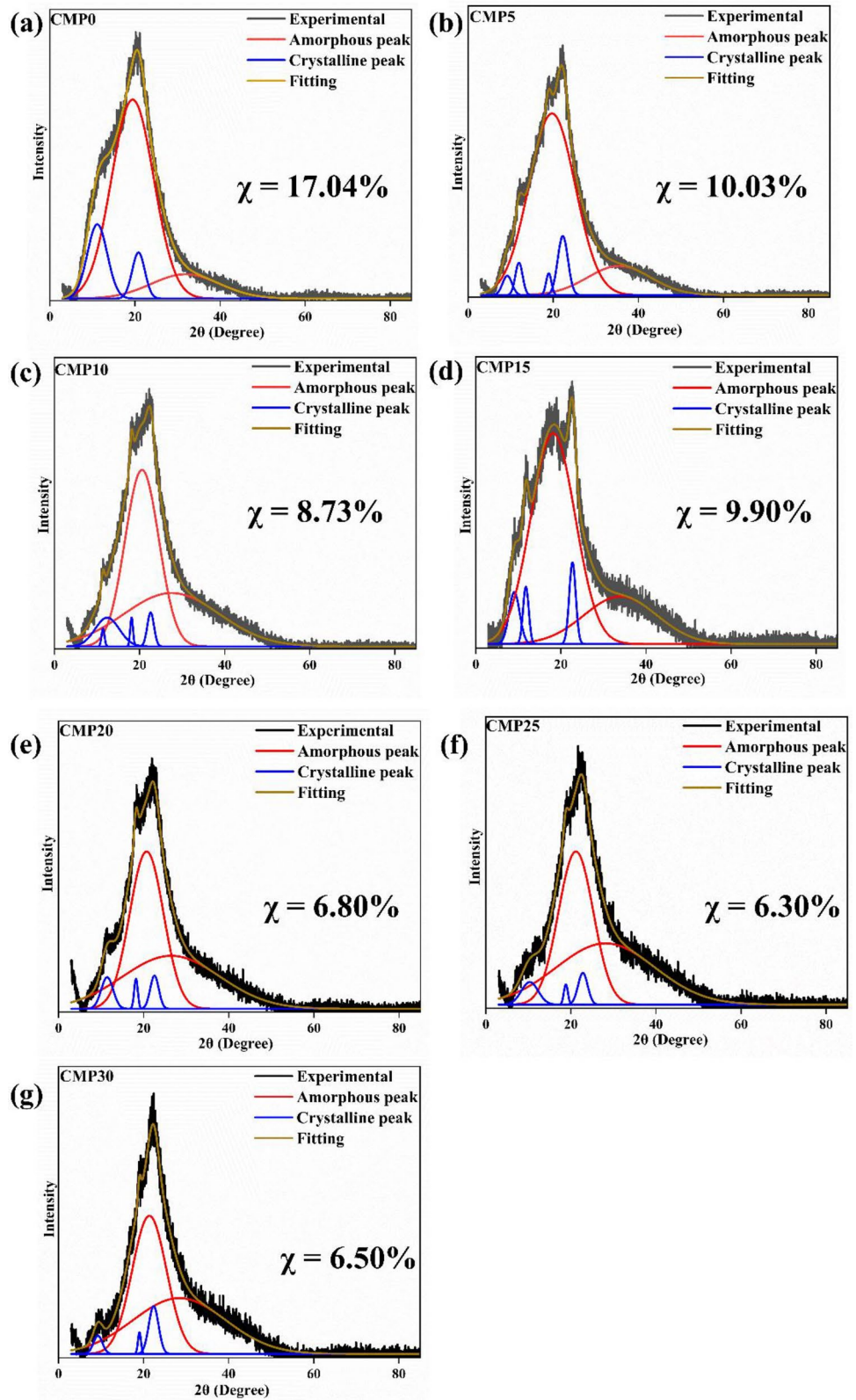
**Fig. 4** **a** Wavenumber variation in the FTIR spectra of synthesized poly-blend electrolyte films **b** Intensity variation in the FTIR spectra of synthesized poly-blend electrolyte films
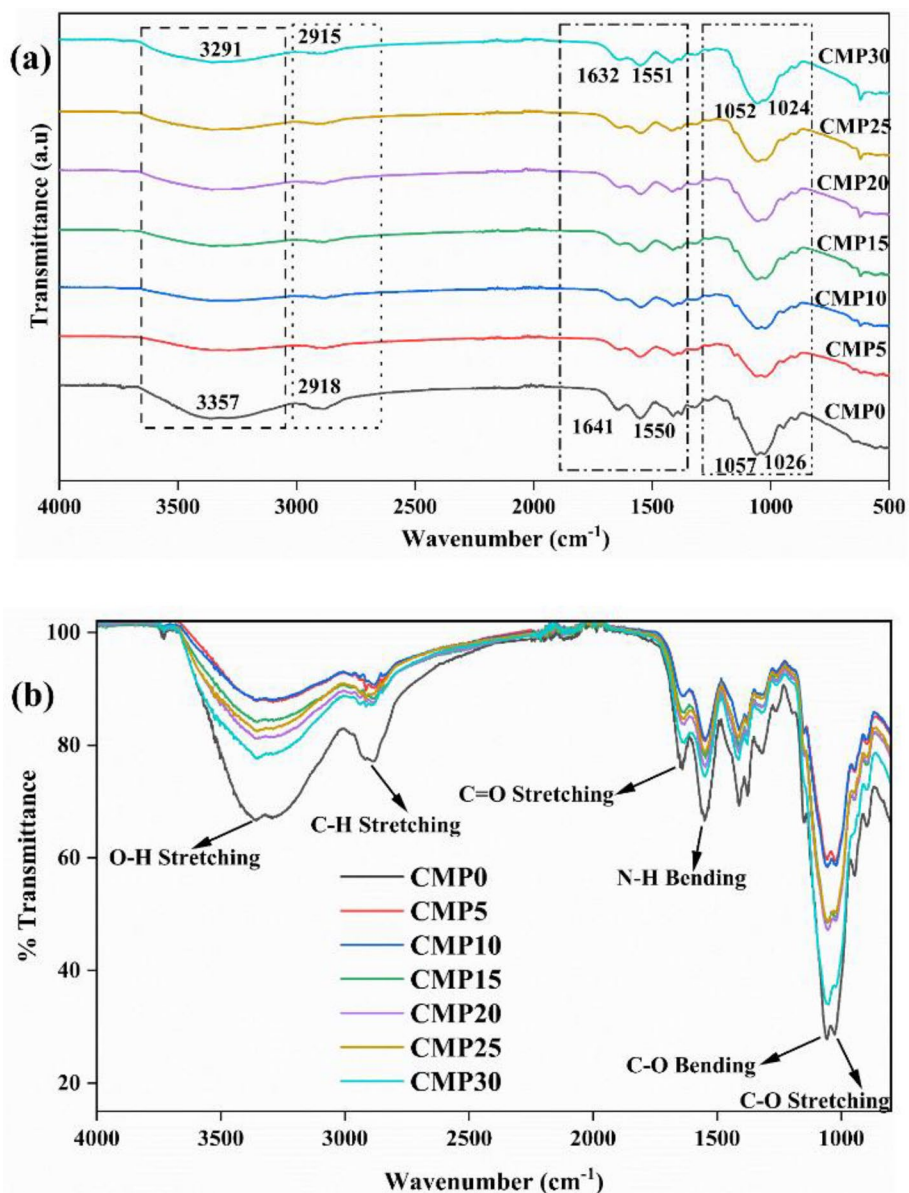
Table 2 FTIR assignments for all the prepared SBPEs

FTIR peak assignment	Wavenumber (cm^{-1})						
	CMP0	CMP5	CMP10	CMP15	CMP20	CMP25	CMP30
-OH stretching	3357	3290	3289	3289	3290	3290	3291
C-H stretching	2918	2915	2882	2890	2886	2916	2915
C=O stretching	1641	1638	1632	1632	1632	1641	1632
-NH bending	1550	1548	1547	1548	1548	1548	1551
C-O bending	1057	1058	1056	1056	1055	1052	1052
C-O stretching	1026	1023	1021	1022	1022	1023	1024

Fig. 5 Probable interaction scheme of Mg(ClO₄)₂ with poly-blend CS:MC
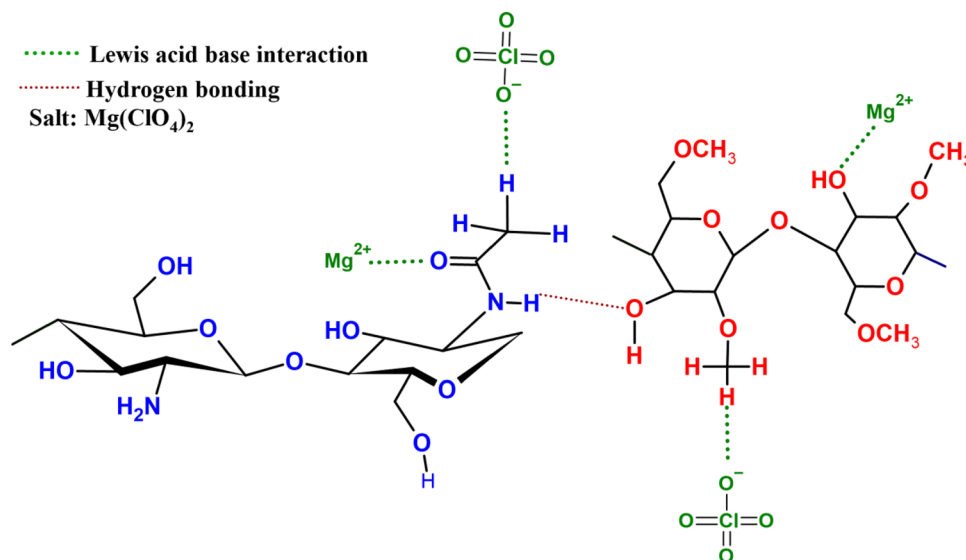
base. The formation of the ion–dipole Mg^{2+}.......OH complex is indicated by a change in the wavenumber of the -OH band. A Lewis acid and a Lewis base form a coordinate covalent bond, forming a Lewis acid–base adduct [30].

3.3 SEM analysis

Figure 6 displays the SEM micrographs of a pure polymer blend and a blend doped with magnesium perchlorate salt. SEM images can be utilized to understand the morphological features of polymer electrolyte samples.

The surface morphology appeared consistent between the pure and doped blends, displaying a smooth surface texture. No cracks or agglomeration of the salt can be seen, even at higher concentrations. Figure 6 shows the EDS image of the highest conducting polymer electrolyte sample (CMP30). All the distinguishing elements (Mg, Cl, O, and C atoms) corresponding to the CS:MC:Mg(ClO4)2 material show that the sample is homogeneous.

3.4 Thermogravimetric analysis

The thermal stability of the SBPE is a crucial factor to consider in ensuring optimal electrolyte performance. Figure 7 presents the thermograms for the pure blend and the blends doped with various Mg(ClO₄)₂ concentrations. During TGA, the initial weight loss observed in the 30–210 °C temperature range is attributed to the vaporization of occluded moisture. The evaporation of

confined liquids causes a 15% initial mass loss in the pure blend at 150 °C. The pure blend film exhibited significant thermal decomposition at 230 °C, indicating that the film remained stable up to this temperature. The highest conducting film (CMP30) is stable up to 220 °C. When the temperature reaches 220 °C, 75% of the mass remains. The second degradation started at 220 °C. The heavyweight loss may be due to the removal of unreacted free monomers from the polymeric chain. Hence, up to 220 °C, the complete stability of all the materials was observed, with an average mass loss of 25%. Given that electrochemical energy storage devices typically operate at temperatures significantly below 100 °C, our samples fulfill this criterion for thermal stability.

3.5 Impedance study

Figure 8 shows the Nyquist plot for the CS:MC:Mg(ClO₄)₂ SBPE system at ambient temperature. The existence of an inclined spike in the low-frequency region of the Nyquist plot is ascribed to ion blocking occurring at the interface between the electrode and electrolyte [42]. This behavior is represented by a constant phase element (CPE1). The depressed semicircle observed in the high-frequency region of the Nyquist plot can be described by the parallel combination of resistance (R_b) and bulk capacitance (CPE2) [43, 44]. The bulk resistance (R_b) indicates the resistance faced by Mg^{2+} ions within the sample's bulk, whereas the bulk capacitance (CPE2) reflects the
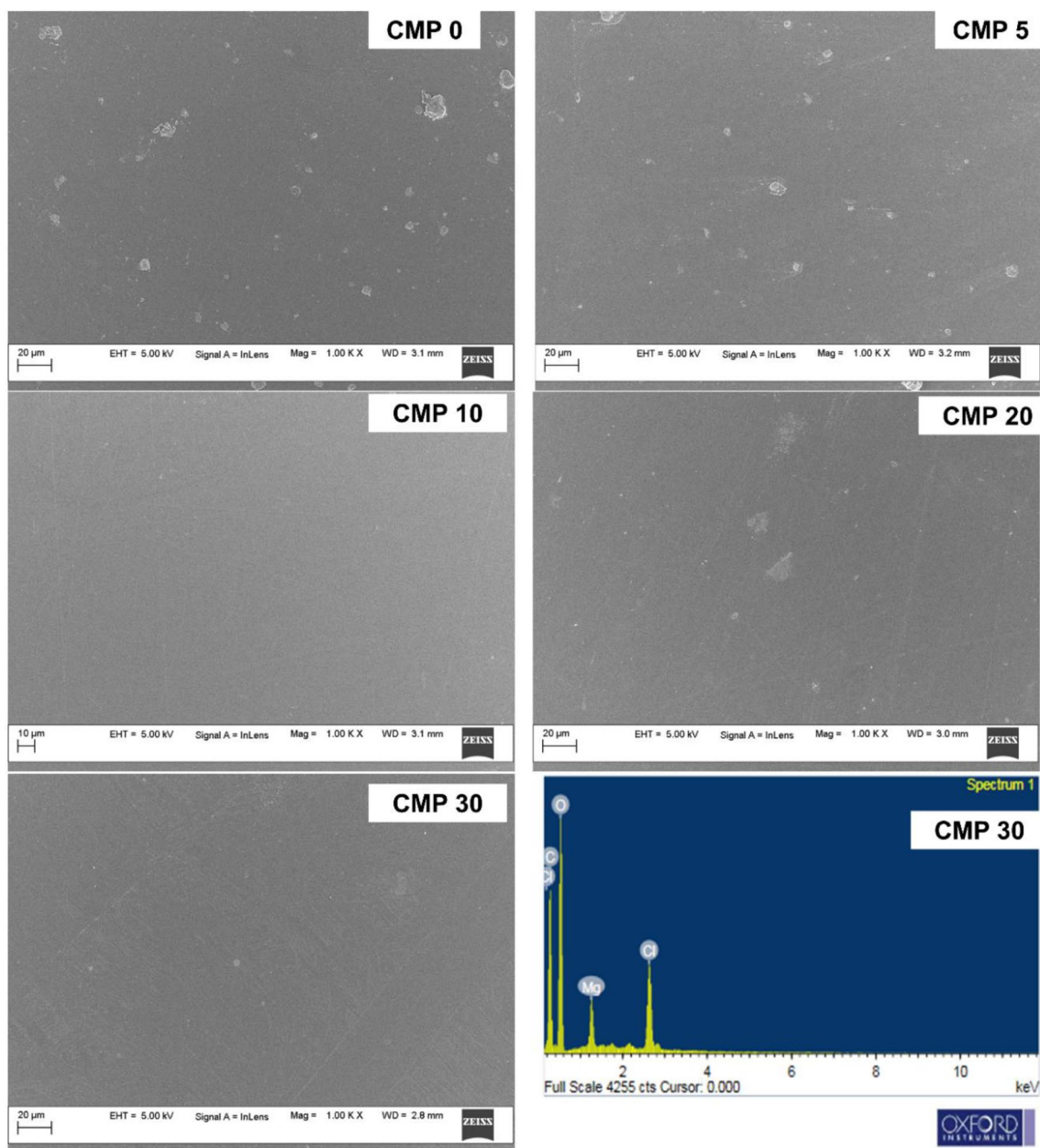
Fig. 6 SEM micrographs of pure poly-blends and blends doped with 5, 10, 20, and 30 wt.% magnesium perchlorate salt along with an EDS image (bottom right) of the highest conducting sample (CMP30)

dipolar polarization of the polymer backbone chain [45]. Ions diffuse through the electrolyte membrane and assemble at the electrolyte/electrode interface as an AC electrical field is applied. Due to the presence of blocking electrodes, the movement of ions across the system is restricted. As a result, the real and imaginary components of the complex impedance can be determined at different frequencies. The R_b value is determined by the intersection of the semicircle with the real axis (Z_r). Equation (1) can be used to calculate the bulk conductivity given the sample's R_b value and the thickness of the SBPE [46]. Table 3 shows the change in bulk conductivity with respect to salt concentration. The ionic conductivity depends upon the type of salt incorporated into the polymer matrix and its extent of dissociation. In polymer networks, the random orientation of dipole moments within the polar side groups leads to a decrease in the diameter of the semicircular
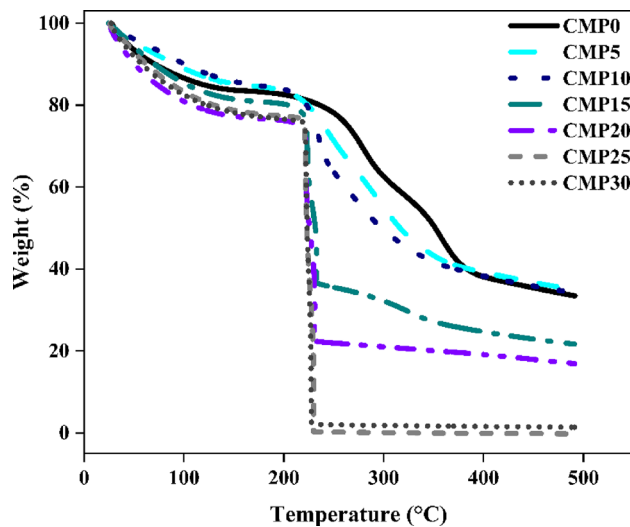
Fig. 7 TG thermograms of CS:MC blends with different concentrations of $Mg(ClO_4)_2$

portion at higher frequencies, especially in samples with increased salt doping in the polymer electrolyte. This reduction signifies the non-capacitive nature of the SBPE, which contributes to more efficient energy storage by minimizing undesired leakage and self-discharge. As a result, the battery's charge can be preserved for longer durations [47]. The undoped blended system has a conductivity of 2.90×10^{-8} S cm^{-1} at room temperature. With the addition of 5 wt% $Mg(ClO_4)_2$ to the CS:MC blend, the conductivity increased by approximately an order of magnitude. The addition of Mg salt to the biopolymer blend matrix led to an increase in conductivity from 10^{-8} to 10^{-6} S cm^{-1}. CMP30 is found to be the highest conducting with an ionic conductivity value of 2.49×10^{-6} S cm^{-1}, which is comparable with the value of 7.23×10^{-6} S cm^{-1} for 30 wt% added KOH salt by Mustafa et al.[48]

3.6 Transport properties

The Nyquist plot was fitted using an appropriate EEC (Fig. 8). As part of the analysis of transport parameters, the carrier concentration (n), carrier mobility (μ), and diffusion coefficient (D) were determined.

$$Z_r = \frac{R + R^2 k_1^{-1} \omega^{p_1} \cos\left(\frac{\Pi p_1}{2}\right)}{1 + 2R k_1^{-1} \omega^{p_1} \cos\left(\frac{\Pi p_1}{2}\right) + R^2 k_1^{-2} \omega^{2p_1}} + \frac{\cos\left(\frac{\Pi p_2}{2}\right)}{k_2^{-1} \omega^{p_2}}$$
(6)

$$Z_i = \frac{R^2 k_1^{-1} \omega^{p_1} \sin\left(\frac{\Pi p_1}{2}\right)}{1 + 2R k_1^{-1} \omega^{p_1} \cos\left(\frac{\Pi p_1}{2}\right) + R^2 k_1^{-2} \omega^{2p_1}} + \frac{\sin\left(\frac{\Pi p_2}{2}\right)}{k_2^{-1} \omega^{p_2}}$$
(7)

The symbols have the usual meaning. The values of p_1 and p_2 lie between 0 and 1. By employing the parameters obtained from the fitting process in Eqs. (6) and (7), the charge transport parameters are estimated using the provided equations, where the symbols retain their conventional meanings:

$$D = \frac{e\left(k_2 \varepsilon_r \varepsilon_o A\right)^2}{\tau_2}$$
(8)

$$\mu = \frac{eD}{k_B T}$$
(9)

$$n = \frac{\sigma}{\mu e}$$
(10)

Table 3 shows the variation in the transport parameters for the CS:MC:$Mg(ClO_4)_2$ SBPE system. Key transport parameters such as mobility (μ), diffusion coefficient (D), and charge density (η) are assessed and scrutinized to determine the primary factors influencing the ionic conductivity of the SBPE. The mobility and diffusion coefficient are high for the samples with 5 wt% salt added to the polymer electrolyte. At low salt concentrations, the salt ions are less likely to interact with the polymer matrix, resulting in the dissociated ions moving freely through the medium. This lack of interaction between the ions and the polymer chains contributes to the elevated mobility and diffusion coefficients observed in the CMP5 sample. As the salt concentration increases, the ions begin to interact more significantly with the polymer chains. This interaction induces segmental motion of the ions in conjunction with the polymer chains, which in turn reduces mobility and diffusion coefficients. Supporting this interpretation, our FTIR studies reveal that the change in wave number is less pronounced for the CMP5 sample than for other polymer electrolyte samples. This indicates that the ion–polymer interactions in the CMP5 sample are less substantial, corroborating our findings related to mobility and diffusion coefficients. Table 3 indicates that as the salt concentration increases, there is a corresponding increase in carrier concentration, except at 20 wt% salt. The observed phenomenon can be attributed to the dissociation of the salt into free ions,

Fig. 8 Nyquist plots for the pristine polymer and Mg(ClO$_4$)$_2$ salt-doped electrolyte samples. Inset: electrical equivalent circuit (EEC) model
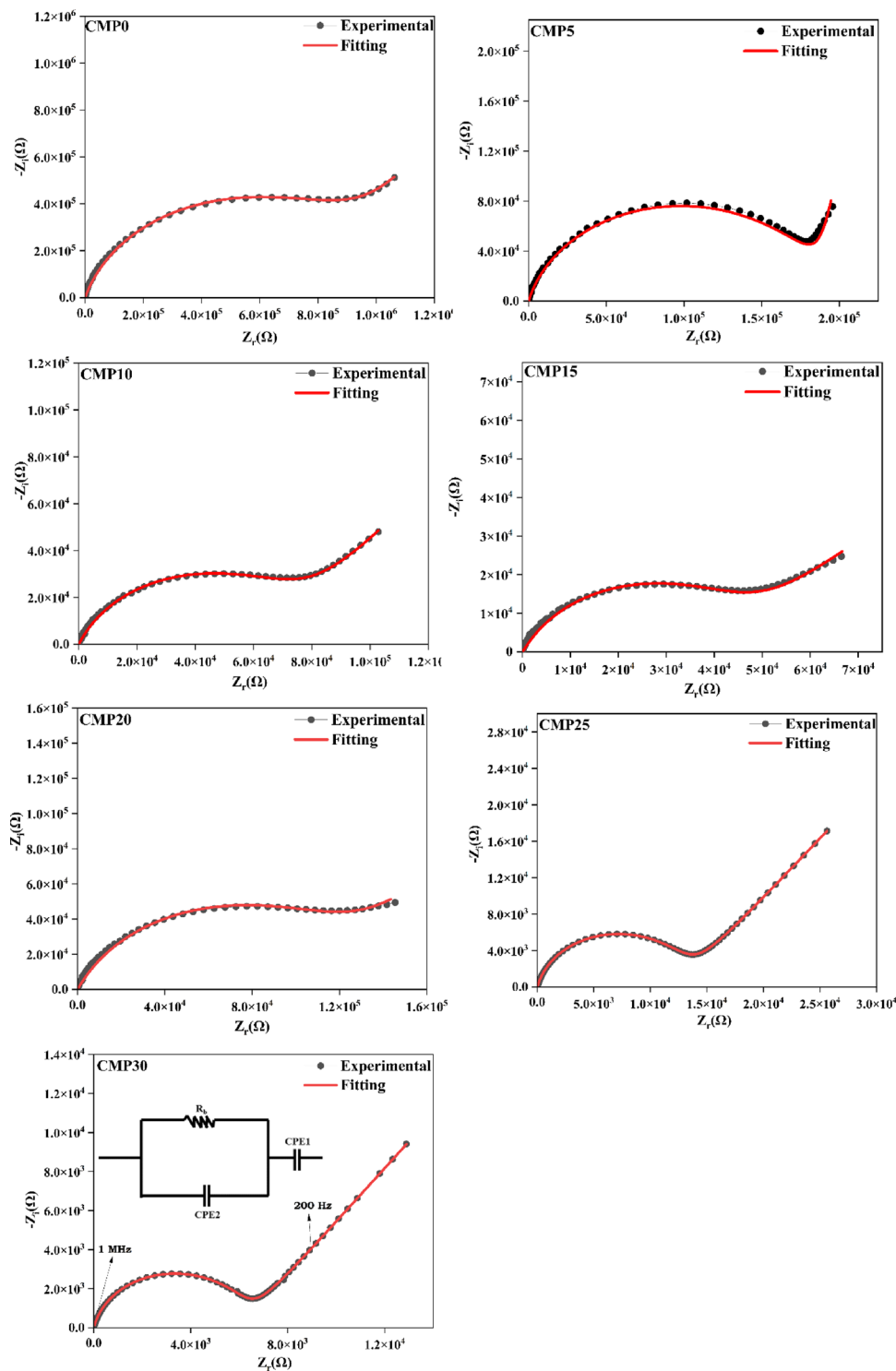
which subsequently form complexes with the -CH and -OH groups present in the blend polymer. This is also evident from the impedance studies, where the conductivity decreases for the CMP20 sample. Table 3 demonstrates a consistent trend in ionic conductivity and carrier concentration across the CMP5 to CMP30 samples, suggesting a substantial influence of charge carrier density on the observed trend in ionic conductivity within the prepared SBPE system.

Table 3 Sample notation, bulk conductivity, transport parameters, and voltage stability window of the pure blend and blend doped with various concentrations of $Mg(ClO_4)_2$ salt

Sample	Bulk resistance (Ω)	Bulk conductivity (S/cm)	n(cm^{-3})	μ(cm^2 V^{-1} s^{-2})	$D\times10^{-2}$ (cm^2 s^{-1})	Electrochemical stability window (V)
CMP0	1,032,831	2.90×10^{-8}	–	–	–	–
CMP5	177,086	1.34×10^{-7}	4.65×10^{10}	8.00	46.70	1.06
CMP10	86,538	1.68×10^{-7}	7.98×10^{12}	0.13	0.34	2.30
CMP15	41,905	3.94×10^{-7}	9.95×10^{13}	0.02	0.06	1.68
CMP20	50,872	1.19×10^{-7}	8.73×10^{12}	0.08	0.22	2.16
CMP25	15,000	1.73×10^{-6}	2.84×10^{14}	0.03	0.09	1.39
CMP30	5813	2.49×10^{-6}	6.63×10^{14}	0.02	0.06	1.92

3.7 I-V characterization

It is crucial to determine the electrochemical stability window (ESW) during the fabrication of an electrochemical device, as it indicates the range where no oxidation or reduction occurs within the polymer electrolyte. In this regard, the ESW of all the synthesized SBPEs was experimentally determined using a Keithley source meter, and the cell layout is shown in Fig. 9. As seen in Fig. 10, the current was insignificant at 1.0 V, indicating that there were no electrochemical processes, and it rapidly increased as the voltage increased to 1.5 V. The ESW for the highest conducting sample (CMP30) was determined by extrapolating the higher voltage linear current along the x-axis [49], which was found to be 1.92 V, which is comparable to the value obtained by Aziz et al. for the plasticized CS polymer electrolyte[50]. The current exhibited a significant increase beyond this voltage, indicating that electrolyte breakdown occurred at the surface of the inert electrodes.

3.8 Transference number measurement (TNM) analysis

3.8.1 Wagner polarization technique

The polarization plot of the SBPEs is shown in Fig. 11. In an SBPE, the total conductivity is due to the involvement of both ions and electrons [51]. In battery or EDLC applications, ions should serve as the primary charge carriers, particularly cations, with minimal electron conductivity ($t_{ion} \gg t_{ele}$) [52].
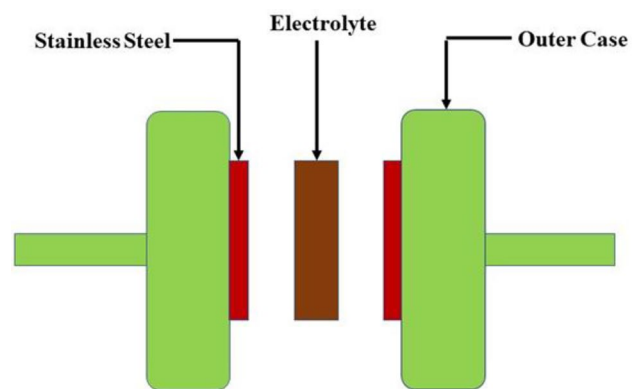
Fig. 9 Typical cell configuration for the I-V and I-t studies

The experimental setup used is shown in Fig. 9. First, the ions and the electrons contribute to the elevated current, after which the current decreases significantly before reaching a constant value. Due to the accumulation of ions at the electrode/electrolyte interface, the current response to a steady state is driven solely by electrons, not ions [53]. SS electrodes, known to block ions, are responsible for this behavior. t_{ion} is computed for all the polymer electrolyte samples using Eq. (3), and for the maximum ion-conducting sample, the t_{ion} is found to be 0.83, which is close to an ideal value of 1, indicating that ions in the highest conducting polymer electrolyte (CMP30) film are the majority charge carrier [54]. The contribution from the magnesium salt's cation and anion is approximately 0.83. The low electronic conductivity justifies the utilization of the prepared electrolytes as both separators and electrolytes in battery applications.
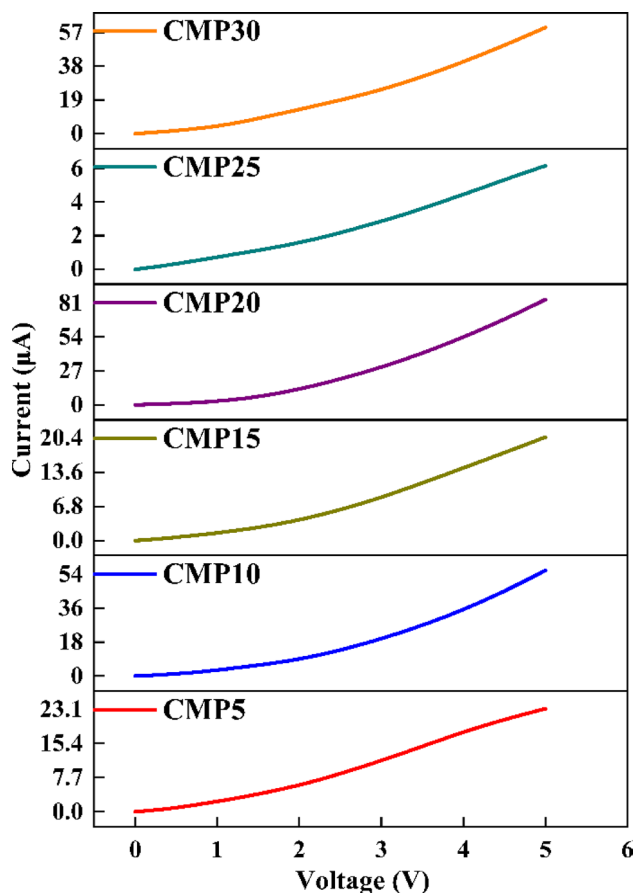
Fig. 10 Graph of the current vs. voltage for the cell composed of SS/[CS:MC]:Mg(ClO$_4$)$_2$/SS
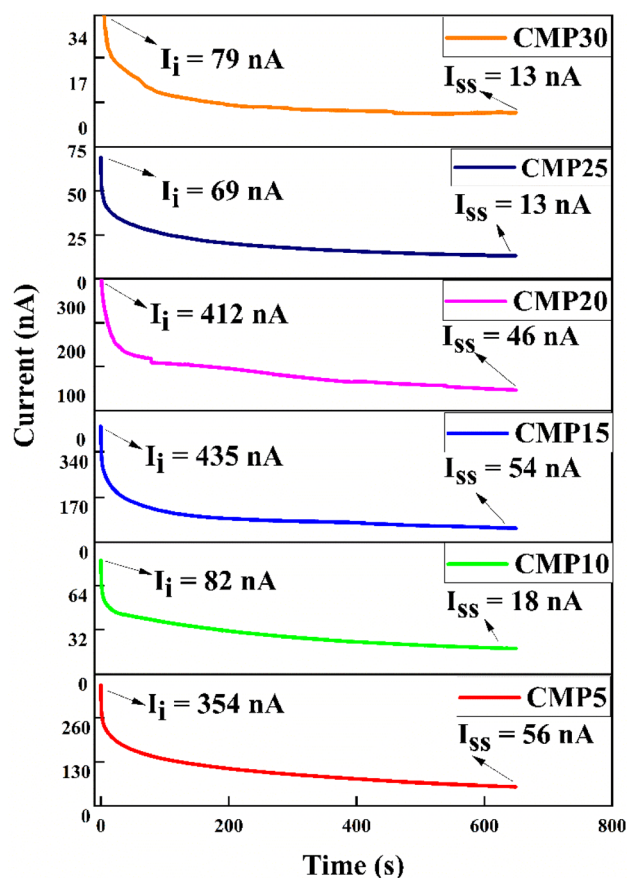
**Fig. 11** A plot of the current versus time for the cell made with SS/[CS:MC]:Mg(ClO$_4$)$_2$/SS

3.9 Cyclic voltammetry (CV)

Researchers commonly employ CV as a useful electro-analytical method for the comparative investigation of electrode material characteristics [55]. It is essential to further analyze the electrochemical reversibility of Mg/Mg^{2+} from an SBPE for application in magnesium-ion batteries. The following two symmetrical cells were used to test the CV of the SBPE containing 30 wt% Mg(ClO$_4$)$_2$, as depicted in Fig. 12.

First cell: SS/CMP30/SS

Second cell: Mg/CMP30/Mg

Both cell types were scanned at a rate of 100 mV s^{-1} from -2.0 V to $+2.0$ V [56]. The first cell's current window is significantly smaller than the second window. Furthermore, the first cell does not show distinct cathodic or anodic peaks, while the second cell shows small redox peaks at -0.6 and $+0.6$ V, respectively. This demonstrates that the SBPE films conduct Mg^{2+} ions reversibly [57].
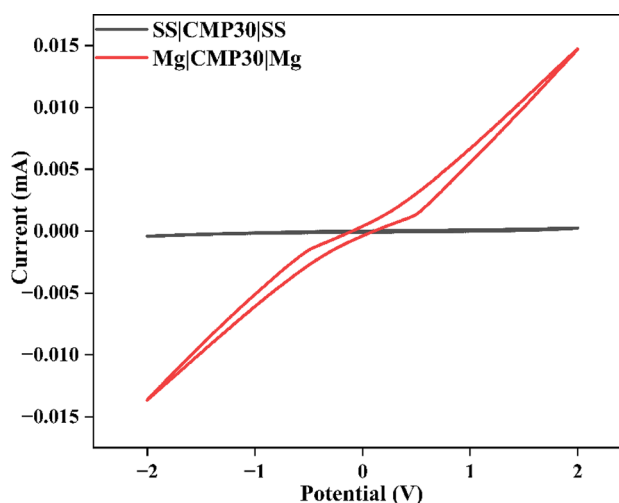
Fig. 12 Cyclic voltammograms (CVs) of the highest ion-conducting polymer electrolyte films

$$Mg^{2+} + 2e^- \leftrightarrow Mg^0$$
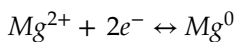
3.9.1 Study of primary magnesium-ion batteries

Figure 13a–d shows the assembly of a primary battery that conducts magnesium ions. The CMP30 polymer electrolyte is sandwiched between a magnesium metal pellet and four different cathode materials in this battery design. In the realm of all-solid-state batteries, the decision regarding the anode material is influenced by the mobile species within the electrolyte, which leads to the selection of a magnesium metal pellet as the anode. The performance of the SBPE was investigated using four different cathode materials to determine how the choice of electrode material affects it.

Adding graphite to cathode materials improves their ability to conduct electricity. In the second cell,

iodine is used as the active material in the cathode. Combining the SBPE with the electrode material increases the surface area where the two materials meet, improving the interaction between them. This reduces the resistance between the electrode and the electrolyte, improving the battery's overall performance.

Table 4 Cell parameters

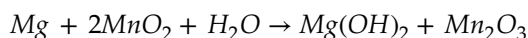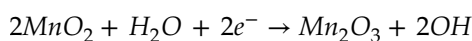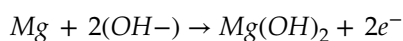| Parameter	Measured values			
	Cell 1	Cell 2	Cell 3	Cell 4
Cell area (cm^2)	1.23	1.23	1.23	1.23
Effective cell diameter (cm)	1.30	1.30	1.30	1.30
Cell thickness (cm)	0.28	0.26	0.34	0.37
Cell weight (g)	0.69	0.71	0.81	0.85
Open-circuit voltage (V))	2.03	1.95	1.50	1.81
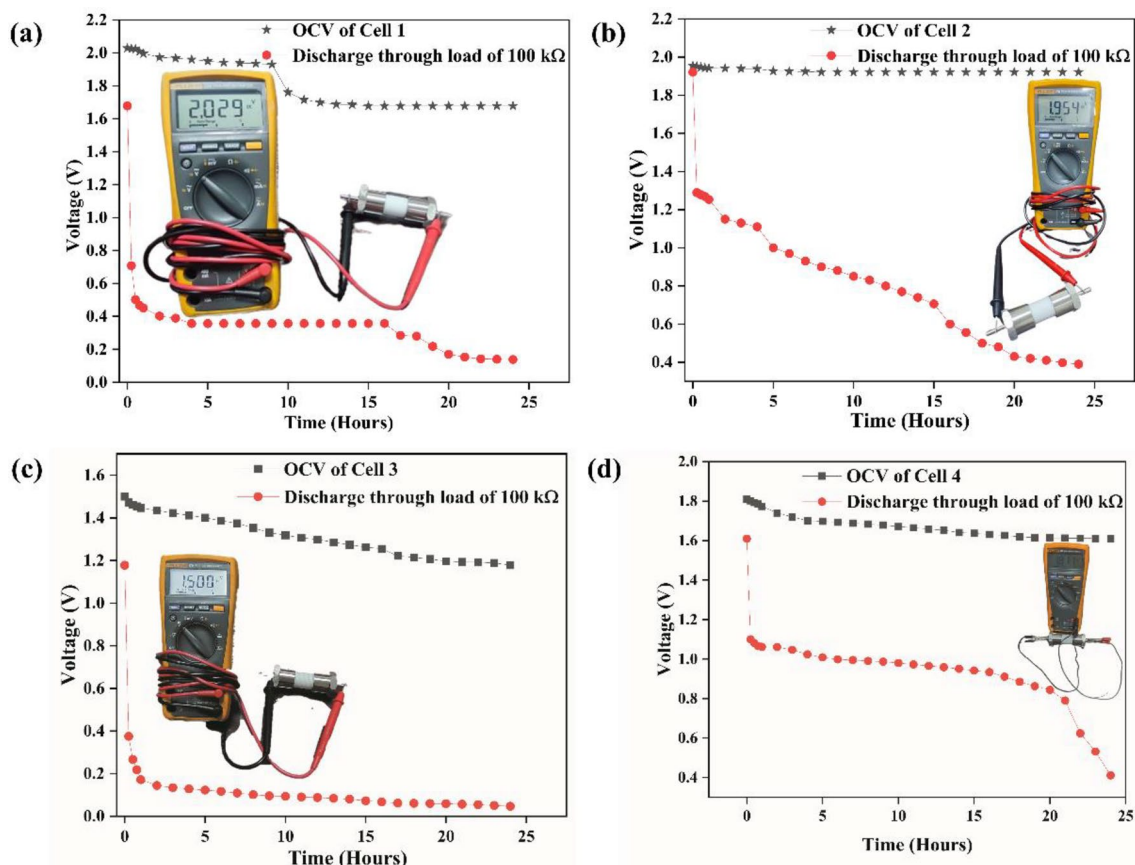
Fig. 13 a The OCV of the first cell (the image of the first cell is presented in the inset). **b** OCV of the second cell (the image of the second cell is displayed in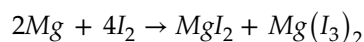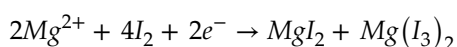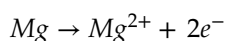 the inset). **c** The OCV of the third cell (the image of the third cell is depicted in the inset). **d** The OCV of the fourth cell (the image of the fourth cell is depicted in the inset)

The cell parameters are listed in Table 4. In the first cell, the initial OCV started at 2.03 V, decreased to 1.68 V, and remained stable for 24 h. During these 24 h, the voltage decreased further to 0.36 V upon applying a load of 100 kΩ. Cell 2's initial OCV began at 1.95 V, decreased to 1.92 V, and remained constant for 24 h. The voltage of the second cell decreased from 1.92 V to 1.3 V when a 100 kΩ resistor was connected. In the third cell, the initial OCV began at 1.5 V and slightly decreased to 1.2 V over 24 h. The voltage decreased steadily for 24 h to 0.09 V after a 100 kΩ load was applied. In the fourth cell, the initial OCV started at 1.81 V, decreased to 1.61 V, and remained stable for 24 h. During these 24 h, the voltage decreased further to 0.41 V upon applying a load of 100 kΩ. The OCV, ESW, and conductivity obtained in the present study are comparable with the results of earlier studies, as depicted in Table 5. This indicates the possible application of the present polymer electrolyte in solid-state batteries. The reaction across the cell components is as follows:
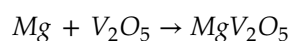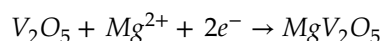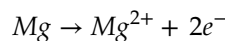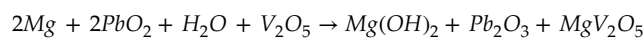
Cell 1:

$$Mg + 2(OH-) \rightarrow Mg(OH)_2 + 2e^-$$

$$2MnO_2 + H_2O + 2e^- \rightarrow Mn_2O_3 + 2OH$$

$$Mg + 2MnO_2 + H_2O \rightarrow Mg(OH)_2 + Mn_2O_3$$

Cell 2:

$$Mg \rightarrow Mg^{2+} + 2e^-$$

$$2Mg^{2+} + 4I_2 + 2e^- \rightarrow MgI_2 + Mg(I_3)_2$$

$$2Mg + 4I_2 \rightarrow MgI_2 + Mg(I_3)_2$$

Cell 3:

$$Mg \rightarrow Mg^{2+} + 2e^-$$

$$V_2O_5 + Mg^{2+} + 2e^- \rightarrow MgV_2O_5$$

$$Mg + V_2O_5 \rightarrow MgV_2O_5$$

Cell 4:

$$Mg \rightarrow Mg^{2+} + 2e^-$$

$$Mg + 2(OH^-) \rightarrow Mg(OH)_2 + 2e^-$$

$$2PbO_2 + H_2O + 2e^- \rightarrow Pb_2O_3 + 2OH^-$$

$$V_2O_5 + Mg^{2+} + 2e^- \rightarrow MgV_2O_5$$

$$2Mg + 2PbO_2 + H_2O + V_2O_5 \rightarrow Mg(OH)_2 + Pb_2O_3 + MgV_2O_5$$
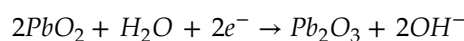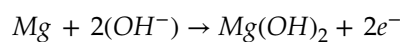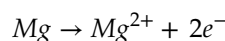
Here, the methylcellulose polymer matrix is the source of hydroxyl (OH$^-$) ions.

4 Conclusion

The solution casting method synthesizes biodegradable SBPE membranes comprising methylcellulose, chitosan, and magnesium perchlorate salt. Chitosan and methylcellulose were used as the biopolymer blend matrix, where ions provided by Mg(ClO$_4$)$_2$

Table 5 Comparison of the maximum ionic conductivity, ESW, and OCV obtained in the present work with those obtained in previous studies

The solid-state electrochemical cell configuration	Maximum ionic conductivity (S cm^{-1})	ESW (V)	OCV (V)	Refs
Mg/(Pectin + Mg(NO$_3$)$_2$)/(MnO$_2$ + Graphite (C))	7.70×10^{-4}	3.80	1.82	[58]
Mg/(Cellulose acetate + Mg(NO$_3$)$_2$)/(MnO$_2$ + C)	9.19×10^{-4}	3.65	2.10	[59]
Mg/(Iota- carrageenan + Mg(NO$_3$)$_2$)/(MnO$_2$ + C)	6.1×10^{-4}	–	2.08	[60]
Mg/(PVA + Mg(NO$_3$)$_2$)/(I$_2$ + C + Electrolyte)	7.36×10^{-7}	–	1.85	[61]
Mg/(Gellan gum + MgCl$_2$)/(MnO$_2$ + C)	2.91×10^{-2}	–	2.39	[62]
Mg/(PVA + PAN + MgCl$_2$)/(MnO$_2$ + C)	1.01×10^{-3}	3.66	2.17	[63]
Mg/(CS + MC + Mg(ClO$_4$)$_2$)/(MnO$_2$ + C + Electrolyte)	2.49×10^{-6}	1.92	2.03	Present work
Mg/(CS + MC + Mg(ClO$_4$)$_2$)/(I$_2$ + C + Electrolyte)	2.49×10^{-6}	1.92	1.95	Present work
Mg/(CS + MC + Mg(ClO$_4$)$_2$)/(V$_2$O$_5$ + C + Electrolyte)	2.49×10^{-6}	1.92	1.50	Present work
Mg/(CS + MC + Mg(ClO$_4$)$_2$)/(PbO$_2$ + V$_2$O$_5$ + C + Electrolyte)	2.49×10^{-6}	1.92	1.81	Present work

participate in the conduction process. The FTIR analysis results indicated the formation of a hydrogen bond between the two polymers and demonstrated good compatibility between the polymers and the magnesium salt via Lewis acid–base interactions. According to the XRD results, the maximum conducting system has the least crystallinity but is less stable above 200 °C. The highest conducting sample exhibited an ionic conductivity of 2.49×10^{-6} S cm^{-1}. I-V analysis revealed that the highest ion-conducting electrolyte with an ESW of 1.92 V is suitable for battery application. The total ionic transference number of the highest conducting electrolyte was 0.83. Cyclic voltammetry revealed an electrochemical equilibrium between the Mg metal and Mg^{2+} ions in the SBPE. The Mg ion electrochemical cells assembled using the highest conducting polymer electrolyte membrane, which acts as an electrolyte and separator, show an open circuit voltage of 2.0 V, thus indicating its practical application. Consequently, the findings suggest that the developed polymer electrolyte exhibits the essential structural and electrochemical properties required for utilization as a separator or electrolyte membrane in magnesium-ion batteries. The battery performance could be further enhanced if suitable electrode materials were tuned to synchronize with the SBPE.

Author contributions

Pradeep Nayak contributed toward conceptualization, methodology, data curation, investigation, and writing-original draft preparation. Ismayil contributed toward methodology, investigation, validation, resources, and supervision. Y. N. Sudhakar contributed toward visualization, resources, data curation, and investigation. M.S. Murari contributed toward resources and investigation.

Data availability

No data or material is provided in this manuscript.

Declarations

Competing interests   The authors declare that they have no known competing financial interests or personal relationships that could have appeared to influence the work reported in this paper.

Consent for publication   The authors hereby consent to publication of the present research in this journal if selected for publication.

Research involving human and animal participants   This article contains no studies with human participants or animals performed by any of the authors.

References

1. A. Zonarsaghar, M. Mousavi-Kamazani, S. Zinatloo-Ajabshir, Sonochemical synthesis of CeVO$_4$ nanoparticles for electrochemical hydrogen storage. Int. J. Hydrog. Energy **47**, 5403–5417 (2022). https://doi.org/10.1016/j.ijhydene.2021.11.183

2. M. Mousavi-Kamazani, S. Zinatloo-Ajabshir, M. Ghodrati, One-step sonochemical synthesis of Zn(OH)$_2$/ZnV$_3$O$_8$ nanostructures as a potent material in electrochemical hydrogen storage. J. Mater. Sci. Mater. Electron. **31**, 17332–17338 (2020). https://doi.org/10.1007/s10854-020-04289-4

3. M. Rezayeenik, M. Mousavi-Kamazani, S. Zinatloo-Ajabshir, CeVO$_4$/rGO nanocomposite: facile hydrothermal synthesis, characterization, and electrochemical hydrogen storage. Appl. Phys. A Mater. Sci. Process. (2023). https://doi.org/10.1007/s00339-022-06325-y

4. S.B. Aziz, O.G. Abdullah, S.A. Hussein, Role of silver salts lattice energy on conductivity drops in chitosan based solid electrolyte: structural, morphological and electrical characteristics. J. Electron. Mater. **47**, 3800–3808 (2018). https://doi.org/10.1007/s11664-018-6250-5

5. J.M. Hadi, S.B. Aziz, S.R. Saeed et al., Investigation of ion transport parameters and electrochemical performance of plasticized biocompatible chitosan-based proton conducting polymer composite electrolytes. Membranes (Basel) **10**, 1–27 (2020). https://doi.org/10.3390/membranes10110363

6. P. Buvaneshwari, T. Mathavan, S. Selvasekarapandian et al., Preparation and characterization of biopolymer electrolyte based on gellan gum with magnesium perchlorate for magnesium battery. Ionics (Kiel) **28**, 3843–3854 (2022). https://doi.org/10.1007/s11581-022-04597-1

7. R. Manjuladevi, M. Thamilselvan, S. Selvasekarapandian et al., blend polymer electrolyte based on poly(vinyl alcohol)-poly (acrylonitrile) with magnesium perchlorate. Solid State Ion. **308**, 90–100 (2017). https://doi.org/10.1016/j.ssi.2017.06.002

8. M.H. Hamsan, S.B. Aziz, M.F.Z. Kadir et al., The study of EDLC device fabricated from plasticized magnesium ion conducting chitosan-based polymer electrolyte. Polym. Test. (2020). https://doi.org/10.1016/j.polymertesting.2020.106714

9. A.K. Arof, M.H. Buraidah, L.P. Teo et al., Characterizations of chitosan-based polymer electrolyte photovoltaic cells. Int. J. Photoenergy (2010). https://doi.org/10.1155/2010/805836

10. R.T. Abdulwahid, S.B. Aziz, M.A. Brza et al., Electrochemical performance of polymer blend electrolytes based on chitosan: dextran: impedance, dielectric properties, and energy storage study. J. Mater. Sci. Mater. Electron. **32**, 14846–14862 (2021). https://doi.org/10.1007/s10854-021-06038-7

11. M.N. Hafiza, A.N.A. Bashirah, N.Y. Bakar, M.I.N. Isa, Electrical properties of carboxyl methylcellulose/chitosan dual-blend green polymer doped with ammonium bromide. Int. J. Polym. Anal. Charact. **19**, 151–158 (2014). https://doi.org/10.1080/1023666X.2014.873562

12. S. Shanmuga Priya, M. Karthika, S. Selvasekarapandian et al., Study of biopolymer I-carrageenan with magnesium perchlorate. Ionics (Kiel) **24**, 3861–3875 (2018). https://doi.org/10.1007/s11581-018-2535-1

13. K.Z. Hamdan, A.S.A. Khiar, Conductivity and dielectric studies of methylcellulose/chitosan-NH$_4$CF$_3$SO$_3$ polymer electrolyte. Key Eng. Mater. **594–595**, 818–822 (2014). https://doi.org/10.4028/www.scientific.net/KEM.594-595.818

14. A.S.A. Khiar, R. Puteh, A.K. Arof, Conductivity studies of a chitosan-based polymer electrolyte. Phys. B Condens. Matter **373**, 23–27 (2006). https://doi.org/10.1016/j.physb.2005.10.104

15. N.A. Nik Aziz, N.K. Idris, M.I.N. Isa, Solid polymer electrolytes based on methylcellulose: FT-IR and ionic conductivity studies. Int. J. Polym. Anal. Charact. **15**, 319–327 (2010). https://doi.org/10.1080/1023666X.2010.493291

16. S. Kiruthika, M. Malathi, S. Selvasekarapandian et al., Conducting biopolymer electrolyte based on pectin with magnesium chloride salt for magnesium battery application. Polym. Bull. **77**, 6299–6317 (2020). https://doi.org/10.1007/s00289-019-03071-9

17. A.R. Polu, R. Kumar, H.W. Rhee, Magnesium ion conducting solid polymer blend electrolyte based on biodegradable polymers and application in solid-state batteries. Ionics (Kiel) **21**, 125–132 (2015). https://doi.org/10.1007/s11581-014-1174-4

18. G. Jo, H. Ahn, M.J. Park, Simple route for tuning the morphology and conductivity of polymer electrolytes: one end functional group is enough. ACS Macro Lett. **2**, 990–995 (2013). https://doi.org/10.1021/mz400468m

19. S.B. Aziz, M.H. Hamsan, R.M. Abdullah, M.F.Z. Kadir, A promising polymer blend electrolytes based on chitosan: methyl cellulose for EDLC application with high specific capacitance and energy density. Molecules (2019). https://doi.org/10.3390/molecules24132503

20. A.A. Abdalrahman, S.B. Aziz, W.O. Karim, EIS and FTIR approaches to study the ion transport parameters and relaxation dynamics of Na^{+1} ion in SPE based on MC polymer inserted with sodium salt. The results Phys **36**, 105439 (2022). https://doi.org/10.1016/j.rinp.2022.105439

21. H.T. Ahmed, V.J. Jalal, D.A. Tahir et al., Effect of PEG as a plasticizer on the electrical and optical properties of polymer blend electrolyte MC-CH-LiBF$_4$ based films. Results Phys. (2019). https://doi.org/10.1016/j.rinp.2019.102735

22. S.S. Abdulkareem, Structural, morphological and electrical properties of chitosan/methylcellulose blend polymer doped with different concentrations of NH$_4$NO$_3$. Mater. Res. Express (2021). https://doi.org/10.1088/2053-1591/ac1d69

23. O.G. Abdullah, R.R. Hanna, H.T. Ahmed et al., Conductivity and dielectric properties of lithium-ion biopolymer blend electrolyte based film. The results Phys **24**, 104135 (2021). https://doi.org/10.1016/j.rinp.2021.104135

24. Y.A.K. Salman, O.G. Abdullah, R.R. Hanna, S.B. Aziz, Conductivity and electrical properties of chitosan—methylcellulose blend biopolymer electrolyte incorporated with lithium tetrafluoroborate. Int. J. Electrochem. Sci. **13**, 3185–3199 (2018). https://doi.org/10.20964/2018.04.25

25. P. Nayak, Y.N. Sudhakar, S. De et al., Optimization of Chitosan: methylcellulose poly-blend to obtain highly amorphous polymer matrix useful for ion transportation. Indian J. Phys. (2023). https://doi.org/10.1007/s12648-023-02684-1

26. P. Nayak, V. Cyriac, S. Hegde, G. Sanjeev, Magnesium ion conducting free-standing biopolymer blend electrolyte films for electrochemical device application. J. Non Cryst. Solids **592**, 121741 (2022). https://doi.org/10.1016/j.jnoncrysol.2022.121741

27. S.B. Aziz, M.H. Hamsan, M.A. Brza et al., Effect of glycerol on EDLC characteristics of chitosan:methylcellulose polymer blend electrolytes. J. Market. Res. **9**, 8355–8366 (2020). https://doi.org/10.1016/j.jmrt.2020.05.114

28. M.H. Hamsan, M.F. Shukur, M.F.Z. Kadir, NH$_4$NO$_3$ as charge carrier contributor in glycerolized potato starch-methyl cellulose blend-based polymer electrolyte and the application in electrochemical double-layer capacitor. Ionics (Kiel) **23**, 3429–3453 (2017). https://doi.org/10.1007/s11581-017-2155-1

29. S.B. Aziz, R.M. Abdullah, Crystalline and amorphous phase identification from the tanδ relaxation peaks and impedance plots in polymer blend electrolytes based on [CS:AgNt]x:PEO(x–1) (10 ≤ x ≤ 50). Electrochim. Acta **285**, 30–46 (2018). https://doi.org/10.1016/j.electacta.2018.07.233

30. B.N. Nadirah, C.C. Ong, M.S.M. Saheed et al., Structural and conductivity studies of polyacrylonitrile/methylcellulose blend based electrolytes embedded with lithium iodide. Int. J. Hydrog. Energy **45**, 19590–19600 (2020). https://doi.org/10.1016/j.ijhydene.2020.05.016

31. O.G.H. Abdullah, R.R. Hanna, Y.A.K. Salman, Structural and electrical conductivity of CH:MC biopoly-blend films: optimize the perfect composition of the blend system. Bull. Mater. Sci. **42**, 1–7 (2019). https://doi.org/10.1007/s12034-019-1742-3

32. A. Zulkifli, M.A. Saadiah, N.F. Mazuki, A.S. Samsudin, Characterization of an amorphous materials hybrid polymer electrolyte based on a LiNO$_3$-doped, CMC-PVA blend for application in an electrical double layer capacitor. Mater. Chem. Phys. **253**, 123312 (2020). https://doi.org/10.1016/j.matchemphys.2020.123312

33. S.B. Aziz, M.H. Hamsan, R.M. Abdullah et al., Protonic EDLC cell based on chitosan (CS): methylcellulose (MC) solid polymer blend electrolytes. Ionics (Kiel) **26**, 1829–1840 (2020). https://doi.org/10.1007/s11581-020-03498-5

34. S.B. Aziz, M.F.Z. Kadir, Z.H.Z. Abidin, Structural, morphological and electrochemical impedance study of CS: LiTf based solid polymer electrolyte: reformulated arrhenius equation for ion transport study. Int. J. Electrochem. Sci. **11**, 9228–9244 (2016). https://doi.org/10.20964/2016.11.18

35. IEEE Malaysia Section. Power Electronics IE& IAJChapter, IEEE Malaysia Section. (2012). CHUSER 2012 : 2012 IEEE Colloquium on Humanities, Science & Engineering Research: Magellan Sutera Resort, Kota Kinabalu, Sabah, Malaysia. IEEE, 3–4 December 2012

36. F. Faghihzadeh, N.M. Anaya, L.A. Schifman, V. Oyanedel-Craver, Fourier transform infrared spectroscopy to assess molecular-level changes in microorganisms exposed to nanoparticles. Nanotechnol. Environ. Eng. **1**, 1–16 (2016). https://doi.org/10.1007/s41204-016-0001-8

37. M.H. Buraidah, A.K. Arof, Characterization of chitosan/PVA blended electrolyte doped with NH 4I. J. Non Cryst. Solids **357**, 3261–3266 (2011). https://doi.org/10.1016/j.jnoncrysol.2011.05.021

38. S.B. Aziz, M.H. Hamsan, R.M. Abdullah, R.T. Abdulwahid, M.A. Brza, A.S. Marif, M.F. Kadir, Protonic EDLC cell based on chitosan (CS): methylcellulose (MC) solid polymer blend electrolytes. Ionics **26**(4), 1829–1840 (2020). https://doi.org/10.1007/s11581-020-03498-5

39. A. Idris, R. Vijayaraghavan, A. Rana, D. Fredericks, A. Patti, D. Macfarlane, Dissolution of feather keratin in ionic liquids. Green Chem. **15**, 525–534 (2013). https://doi.org/10.1039/C2GC36556A

40. Y. Zhang, W. Zhao, R. Yang, Steam flash explosion assisted dissolution of keratin from feathers. ACS Sustain. Chem. Eng. **3**, 2036–2042 (2015). https://doi.org/10.1021/acssuschemeng.5b00310

41. O.G. Abdullah, Y.A.K. Salman, S.A. Saleem, Electrical conductivity and dielectric characteristics of in situ

prepared PVA/HgS nanocomposite films. J. Mater. Sci. Mater. Electron. **27**, 3591–3598 (2016). https://doi.org/10.1007/s10854-015-4196-4

42. A.R. Polu, R. Kumar, AC impedance and dielectric spectroscopic studies of Mg^{2+} ion conducting PVA-PEG blended polymer electrolytes. Bull. Mater. Sci. **34**, 1063–1067 (2011). https://doi.org/10.1007/s12034-011-0132-2

43. S.B. Aziz, The mixed contribution of ionic and electronic carriers to conductivity in chitosan based solid electrolytes mediated by CuNt salt. J. Inorg. Organomet. Polym. Mater. **28**, 1942–1952 (2018). https://doi.org/10.1007/s10904-018-0862-3

44. S.B. Aziz, E.M.A. Dannoun, M.H. Hamsan et al., Improving edlc device performance constructed from plasticized magnesium ion conducting chitosan based polymer electrolytes via metal complex dispersion. Membranes (Basel) (2021). https://doi.org/10.3390/membranes11040289

45. M.S.M. Misenan, M.I.N. Isa, A.S.A. Khiar, Electrical and structural studies of polymer electrolyte based on chitosan/methyl cellulose blend doped with BMIMTFSI. Mater. Res. Express (2018). https://doi.org/10.1088/2053-1591/aac25b

46. K. Sravanthi, G.S. Sundari, H. Erothu, Development of biodegradable based polymer electrolytes for EDLC application. Optik (Stuttg) (2021). https://doi.org/10.1016/j.ijleo.2020.166229

47. M. Mahalakshmi, S. Selvanayagam, S. Selvasekarapandian et al., Characterization of biopolymer electrolytes based on cellulose acetate with magnesium perchlorate ($Mg(ClO_4)_2$) for energy storage devices. J. Sci. Adv. Mater. Devices **4**, 276–284 (2019). https://doi.org/10.1016/j.jsamd.2019.04.006

48. Mustafa MF, Ridwan NIM, Hatta FF, Yahya MZA (2012) Effect of dimethyl carbonate plasticizer on ionic conductivity of methyl cellulose-based polymer electrolytes (Pengaruh Pemplastik Dimetil Karbonat ke atas Kekonduksian Ionik Elektrolit Polimer Berasaskan Metil Selulos)

49. M.K. Song, Y.T. Kim, Y.T. Kim et al., Thermally stable gel polymer electrolytes. J. Electrochem. Soc. **150**, A439 (2003). https://doi.org/10.1149/1.1556592

50. A.S.F.M. Asnawi, S.B. Aziz, M.M. Nofal et al., Glycerolized Li^+ ion conducting chitosan-based polymer electrolyte for energy storage EDLC device applications with relatively high energy density. Polymers (Basel) (2020). https://doi.org/10.3390/polym12061433

51. E.M.A. Dannoun, S.B. Aziz, M.A. Brza et al., The study of plasticized solid polymer blend electrolytes based on natural polymers and their application for energy storage EDLC devices. Polymers (Basel) **12**, 1–19 (2020). https://doi.org/10.3390/polym12112531

52. S.B. Aziz, I. Brevik, M.H. Hamsan et al., Compatible solid polymer electrolyte based on methyl cellulose for energy storage application: Structural, electrical, and electrochemical properties. Polymers (Basel) **12**, 1–19 (2020). https://doi.org/10.3390/polym12102257

53. T. Maheshwari, K. Tamilarasan, S. Selvasekarapandian et al., Investigation of blend biopolymer electrolytes based on Dextran-PVA with ammonium thiocyanate. J. Solid State Electrochem. (2020). https://doi.org/10.1007/s10008-020-04850-5

54. M.M. Nofal, J.M. Hadi, S.B. Aziz et al., A study of methylcellulose based polymer electrolyte impregnated with potassium ion conducting carrier: impedance, eec modeling, ftir, dielectric, and device characteristics. Materials (2021). https://doi.org/10.3390/ma14174859

55. S. Zinatloo-Ajabshir, M.H. Esfahani, C.A. Marjerrison et al., Enhanced electrochemical hydrogen storage performance of lanthanum zirconium oxide ceramic microstructures synthesized by a simple approach. Ceram. Int. **49**, 37415–37422 (2023). https://doi.org/10.1016/j.ceramint.2023.09.067

56. M. Ramaswamy, T. Malayandi, S. Subramanian et al., Development and study of solid polymer electrolyte based on polyvinyl alcohol: $Mg(ClO_4)_2$. Polym. Plast. Technol. Eng. **56**, 992–1002 (2017). https://doi.org/10.1080/03602559.2016.1247280

57. R. Manjuladevi, S. Selvasekarapandian, M. Thamilselvan et al., A study on blend polymer electrolyte based on poly(vinyl alcohol)-poly (acrylonitrile) with magnesium nitrate for magnesium battery. Ionics (Kiel) **24**, 3493–3506 (2018). https://doi.org/10.1007/s11581-018-2500-z

58. S. Kiruthika, M. Malathi, S. Selvasekarapandian et al., Eco-friendly biopolymer electrolyte, pectin with magnesium nitrate salt, for application in electrochemical devices. J. Solid State Electrochem. **23**, 2181–2193 (2019). https://doi.org/10.1007/s10008-019-04313-6

59. M. Mahalakshmi, S. Selvanayagam, S. Selvasekarapandian et al., Magnesium ion-conducting solid polymer electrolyte based on cellulose acetate with magnesium nitrate ($Mg(NO_3)_2 \cdot 6H_2O$) for electrochemical studies. Ionics (Kiel) **26**, 4553–4565 (2020). https://doi.org/10.1007/s11581-020-03615-4

60. S. Shanmuga Priya, M. Karthika, S. Selvasekarapandian, R. Manjuladevi, Preparation and characterization of polymer electrolyte based on biopolymer I-Carrageenan with magnesium nitrate. Solid State Ion. **327**, 136–149 (2018). https://doi.org/10.1016/j.ssi.2018.10.031

61. A.R. Polu, R. Kumar, Preparation and characterization of pva based solid polymer electrolytes for electrochemical cell applications. Chin. J. Polym. Sci. **31**, 641–648 (2013). https://doi.org/10.1007/s10118-013-1246-3

62. P. Buvaneshwari, T. Mathavan, S. Selvasekarapandian et al., Biopolymer electrolyte based on gellan gum with magnesium chloride for magnesium battery. Ionics (2021). https://doi.org/10.1007/s11581-022-04597-1

63. R. Manjuladevi, M. Thamilselvan, S. Selvasekarapandian et al., Preparation and characterization of blend polymer electrolyte film based on poly(vinyl alcohol)-poly(acrylonitrile)/MgCl$_2$ for energy storage devices. Ionics (Kiel) **24**, 1083–1095 (2018). https://doi.org/10.1007/s11581-017-2273-9

Publisher's Note Springer Nature remains neutral with regard to jurisdictional claims in published maps and institutional affiliations.